POLITECNICO
MILANO 1863

Nuclear Engineering Division, Department of Energy
Introduction to Nuclear Engineering
A.Y. 2024/2025

Professor: Marco Enrico Ricotti

WG9: Space Reactor KRUSTY

Sodium Subgroup

Name	Person Code	Email
Cristian Mandolini	10724204	cristian.mandolini@mail.polimi.it
Adam Lakrad	10727361	adam.lakrad@mail.polimi.it
Chiara Conte	10703587	chiara.conte@mail.polimi.it
Emanuele Gallo	10766758	emanuele.gallo@mail.polimi.it
Valeria Forleo	10923422	valeria1.forleo@mail.polimi.it
Francesca Giulia Cicchi	10765800	francescagiulia.cicchi@mail.polimi.it
Joshua Kristopher Smith	10868169	joshuakristopher.smith@mail.polimi.it

Date: 31/01/2025

Contents

List of Figures

List of Tables

1 Introduction

The KRUSTY (Kilopower Reactor Using Stirling Technology) is an experimental fission reactor developed by NASA and the U.S. Department of Energy for in-space application. Highly Enriched Uranium-235 is used as fuel, liquid sodium as working fluid, and Stirling engines to generate electricity. While many uses for the KRUSTY were considered, such as energy generation in orbit or being coupled with an electric propulsion unit, the main application currently being considered is power generation for a future crewed base on the Lunar South Pole. In fact, current plans by NASA involve creating a Human Outpost in one of the craters of the Lunar South Pole, such as the Shackleton Crater. Due to their particular location, the peaks along the craters' rim are exposed to almost continual sunlight, while the interior is perpetually in shadow. The low-temperature interior of these craters allows for the presence of water ice beneath the Lunar surface. Ice can be extracted and purified to obtain drinkable water, which can be used to sustain the astronauts inhabiting the Outpost. The fact that these craters receive almost no sunlight, means that solar arrays cannot be used for power generation. For this reason, a nuclear reactor was chosen as the main power source for the base, as it can operate regardless of environmental conditions.

1.1 Mission high level requirements

The type of mission coupled with the harsh environment generate the set of high level requirements shown Table 1. Every requirement is identified by a unique ID, in accordance with ECSS standards.

ID	High Level Requirement
REQ-01	The reactor **shall** produce sufficient energy to fulfill the energy needs of the human outpost on the lunar surface.
REQ-02	The reactor **shall** operate continuously for up to 12 years.
REQ-03	The reactor **shall** provide energy for the whole duration of the mission without interruptions.
REQ-04	The reactor **shall** be kept safe in all phases of the mission, including testing and launch.
REQ-05	The reactor **shall** be as lightweight and compact as possible.
REQ-06	The reactor **shall** use U-235 as fuel to comply with international regulations.
REQ-07	The reactor **shall** be able to operate on the Moon and **shall** be able to withstand the harsh environment of the Lunar South Pole.

Table 1: Requirements of the mission.

1.2 Design of the KRUSTY

The reactor features two circuits: a primary hot one directly in contact with the reactor and a secondary cold one using helium that dissipates heat through a radiator. The two circuits exchange heat via a Stirling engine, which generates rotational kinetic energy using the temperature difference between the two fluids. Three different models were considered, and their datasheets are reported in Table 2. Using this data, each model was modeled and analyzed, and then a trade-off analysis was performed.

Parameter	Symbol	**RE-1000**	**EG-1000**	**SDPE**
Hot side temperature	T_{hot}	873 K	773 K	650 K
Cold side temperature	T_{cold}	303 K	323 K	325 K
Efficiency	η	0.29	0.20	0.22
Frequency	f	30 Hz	50 Hz	100 Hz
Mean operating pressure	P_m	7 MPa	1 MPa	15 MPa
Output power	W_{out}	1 kW_e	1 kW_e	25 kW_e

Table 2: Datasheet of the RE-1000 Stirling Engine. [11]

Due to the extreme environmental conditions the KRUSTY has to operate in, liquid water cannot be used as a working fluid. Instead, other fluids, such as sodium, potassium, and lithium, were considered. To perform

the sizing, **liquid sodium** was considered, which has a very wide range of operational temperatures and a low neutron absorption cross section [12], as highlighted in Table 3.

Parameter	Symbol	Value
Melting temperature	T_m^{Na}	$98°C$ [12]
Boiling temperature	T_b^{Na}	$892°C$ [12]
Density	ρ	$927\ kg/m^3$ [4]
Viscosity	ν	$0.0007\ Pa \cdot s$ [4]
Scattering cross section	σ_A	$3.28\ barn$ [13]
Absorption cross section	σ_S	$0.53\ barn$ [13]

Table 3: Properties of liquid sodium.

1.3 Environment: Shackleton Crater

As already mentioned, the reactor shall operate in the Shackleton Crater on the Lunar South Pole. The environmental conditions of the crater are highlighted in Table 4.

Parameter	**Value**
Surface Temperature	$175\ K$
Deep Space Temperature	$2.7\ K$
Solar Constant (average)	$1358\ kW/m^2$
Lunar Gravity	$1.625\ m/s^2$

Table 4: Environmental parameters of Shackleton Crater. [11]

2 Sizing

2.1 Steady-State Model

2.1.1 Assumptions

To perform the sizing, the following assumptions were made:

- The nominal power output of the reactor is $5\,kW_{th}$.
- The Stirling engine is assumed to be ideal.
- Helium, working fluid of the Stirling engine, is assumed to be an ideal gas.

2.1.2 Heat Pipes Overview

The heat pipes are made up of the following configuration. An inner vapor region where gaseous sodium flows from the heat source (reactor) to the heat sink (Stirling Engines) highlighted in Figure 1 and Figure 2. Once the vapor reaches the condenser section, the fluid cools back to liquid form within the wick, where it is transported back towards the heat source through the use of capillary forces. Gravitational forces can be used to help or hinder the motion of the fluid, depending on the orientation of the pipe.

$$\Delta p_{\text{evap}} + \Delta p_v + \Delta p_{\text{cond}} + \Delta p_{\ell,\text{flow}} + \Delta p_{\ell,g} \leq \Delta p_{\text{cap,max}} \tag{1}$$

In order to size the pipe configuration, the following equations needed to be satisfied. The total pressure drops need to be less than the max capillary pressure, which is defined here:

$$\Delta p_{\text{cap,max}} = \frac{2\sigma}{R_{\text{eff}}} \tag{2}$$

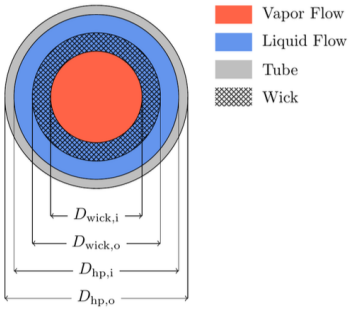

Figure 1: Heat Pipe configuration [6]

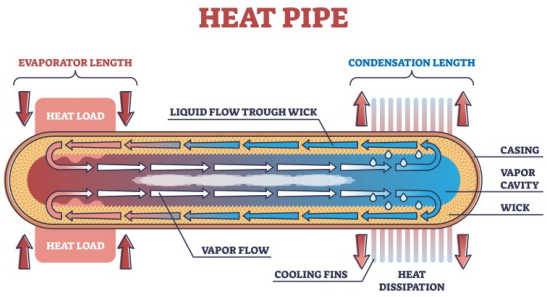

Figure 2: Heat Pipe configuration (side view)

Where the σ is the surface tension and R_{eff} is the effective pour radius. By neglecting the pressure drop from condensation, evaporation, and vapor we can focus on the pressure drop on the liquid from friction (darcy-weisbach). They are represented by both equations 4and 3.

$$\Delta p_{\ell,g} = \rho_\ell g L_{\text{pipe}} \sin\theta \tag{3}$$

$$\Delta p_{l,\text{flow}} = \frac{L_{\text{eff}} \dot{Q}_{pipe} \mu_l}{K h_{\text{lat}} \rho_l A_l} \tag{4}$$

Both of the equations are dependent on the density of the liquid and length of the pipe . (i.e effective length is taken to be length of the pipe $L_{\text{pipe}} = L_{\text{eff}}$). The wick area through which the liquid flows through , A_l, can be sized by combining the the limiting case of equation of 1.

$$A_l = \frac{L_{\text{eff}} \dot{Q}_{\text{pipe}} \mu_l}{K h_{\text{lat}} \rho_l \left(\Delta P_{\text{cap}} - \Delta P_g\right)} \tag{5}$$

Equation 5 shows that the area of the wick is mainly controllable by the length of the tube, the heat load transported to the tube, and the type of working fluid (i.e h_{lat},ρ_l, μ_l).
For the vapor section of the pipe, the area is mainly restricted by the limits from entrainment and sonic heat transfer. They are represented by equations 7 and 6.

$$\dot{Q}_{sonic} = A_v \rho_v h_{lat} \sqrt{\frac{\gamma R T_v}{2(\gamma+1)}} \tag{6}$$

$$\dot{Q}_{\text{max,ent}} = A_v h_{\text{lat}} \left(\frac{2\sigma\rho_v}{R_{\text{pore}}}\right)^{1/2} \tag{7}$$

Other limits exist such as from boiling and viscosity but for sodium heat pipe configurations tend to be less restrictive than sonic and entrainment [14]. This can be seen from figure 3. Based on these results, it was determined that it was only necessary to model sonic, entrainment, and viscosity. The viscosity heat limit is modeled using the equation 8.

$$\dot{Q}_{\text{max, vis}} = \frac{A_v^2 h_{\text{lat}} \rho_v p_v}{16\pi\mu_v L_{\text{eff}}} \tag{8}$$

In this equation, A_v represents the characteristic area of the vapor flow, h_{lat} is the latent heat of vaporization, ρ_v denotes the density of the vapor, and p_v is the vapor pressure. The term μ_v corresponds to the dynamic viscosity of the vapor.
The definitions and values

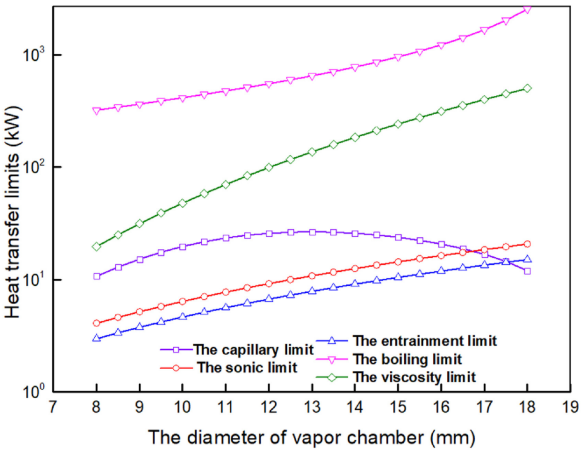

Figure 3: Heat Limits vs vapor chamber diameter of Sodium heat pipe [14]

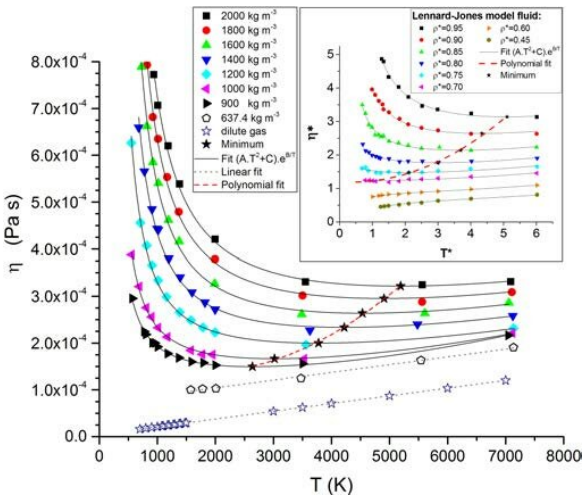

Figure 4: Dynamic viscosity of Sodium for different temperatures and density [10]

2.1.3 Method and results for sizing Heat pipes

It is assumed that the total heat from reactor, 5 KW, is evenly distributed to each of the pipes. This heat which is denoted as $\dot{Q}_{pipe}$, is used within equation 5 to find the wick area. The size of the total cross sectional area of the pipe is the sum of the vapor section, the wick section, and the outer thickness of the pipes. The outer diameter of the vapor and wick of the pipe was varied using common nominal values found in throughout the literature review. The area of the vapor was then determined by subtracting the wick area from the total area of the pipe using equation 5.

Symbol	Value	Name
$\sigma\ [N/m]$	0.185	Surface tension
$R_{\text{eff}}[m]$	20×10^{-6}	Effective pore radius
$\rho_l\ kg/m^3$	741.2	Liquid density of sodium
$\rho_v\ kg/m^3$	0.259	Vapor density of sodium
$g\ [m/s^2]$	1.625	Gravitational acceleration of the Moon
L_{pipe} [m]	1	Pipe length
$\theta\ [^o]$	0,-90,90	Inclination angle of the pipe
$p_v\ [Pa]$	95500	Vapor pressure of sodium
N	8	Number of pipes
μ_l	0.00018	Dynamic viscosity of the liquid
μ_v	$1.897581345 \times 10^{-5}$	Dynamic viscosity of the vapor
$K\ [m^2]$	10^{-10}	Wick permeability
$h_{\text{lat}}\ [J/kg]$	3863457.53	Latent heat of vaporization
$T_w\ [K]$	1047.15	Working temperature

Table 5: Values used based on T_w.

Other constant values used in the equations above, are shown in table 5. The table provides definitions and values for the symbols used in the model. The surface tension (σ), effective pore radius (R_{eff}), liquid density (ρ_l), and wick permeability (K) are taken from *The liquid-conduction, vapor-flow heat pipe model in Sockeye*. The pipe length (L_{pipe}) and working temperature (T_w) are taken from *Preliminary architecture of nuclear space reactor for a lunar base*. Lastly, the latent heat of vaporization (h_{lat}) is based on data from *Tables of thermodynamic properties of sodium*. are a function of the working temperature of the fluid. They They are taken from tabulate values from *Tables of thermodynamic properties of sodium* [3]. For the dynamic viscosity of the vapor, was calculated using an empirical formula based on the temperature of the working fluid taken from *design of*

high-temperature sodium heat pipes [14]. The formula is shown here.

$$\mu_g = 6.083 \times 10^{-9} T + 1.2606 \times 10^{-5} \tag{9}$$

The value for the dynamic viscosity of liquid sodium was taken from data obtained in figure 4 [10].
In order to then size the for the area of the vapor region, a suitable radius for the vapor region must satisfy the sonic and entrainment limits within the pipe.

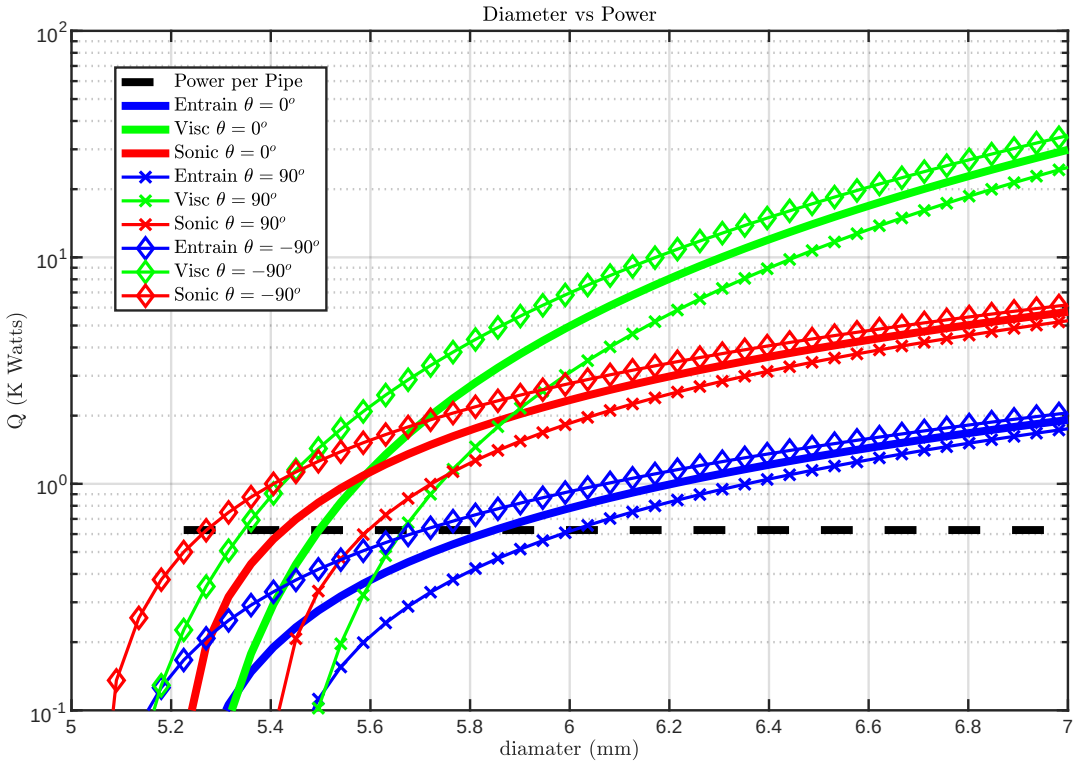

Figure 5: Heat Limits for 8 pipes

Figure 3 shows how the diameter vs power transfer limits for the pipes. The results are obtained for different orientations of diffferent vertical and horizontal configurations. The entrainment limit is generally the most dominating case followed by sonic and the viscous. However at very small diameters near 5.6 mm viscous limit is more dominate than the sonic limit. In all cases $\theta = 90^o$ allowed for a smaller pipe to be developed. Accounting for a margin of saftey the current sizing configuration for the outer diameter, vapor area, and wick area is shown in table 6. These values remain suitable small, while staying far away from any of the three limits presented in figure 5.

#Pipes	Outer Diameter (mm)	Vapour Area (mm^2)	Wick Area (mm^2)	Total Area (mm^2)
8	6.92	13.80	22.71	36.51

Table 6: Final configuration

2.1.4 Stirling Engine

Introduction Here it is reported a brief introduction to the Stirling engine and its cycle. The main assumptions are the following.

- The engine is modeled as a closed system, therefore exchanging no mass with the environment but only heat and work.

- The working fluid is modeled as an ideal gas.
- The transformations that make up the cycle are considered ideal.
- The walls of the engine will be perfectly adiabatic, meaning no heat losses will occur.

Under these hypotheses, the cycle, as shown in Figure 6, is composed of four transformations:

1. **Isothermal expansion 1-2.**
2. **Isochoric transformation 2-3.**
3. **Isothermal compression 3-4.**
4. **Isochoric transformation 4-1.**

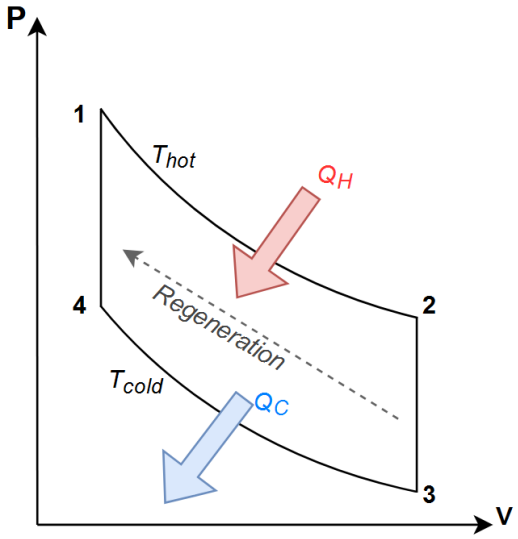

Figure 6: Ideal Stirling cycle in the P-V plane.

The first expansion is driven by the heat Q_H that comes from an external source, in this case the reactor core. The transformation is governed by the following equation:

$$Q_H = M R^* T_{hot} \ln(r) \tag{10}$$

Where M is the mass of the gas in the system, R^* is the specific gas constant, T_{hot} is the hot side temperature and $r = V_{max}/V_{min}$ is the compression ratio. The transformation 2-3 will generate heat according to following equation:

$$Q_{reg} = M C_v (T_{hot} - T_{cold}) \tag{11}$$

Where C_v is the specific heat ratio at constant volume and T_{cold} is the cold side temperature. This heat is transferred to 4-1 through the use of a regenerator. In the ideal case, this component will have unitary efficiency, meaning that all the heat is transferred without losses. In the real case, however, there will inevitably be heat losses that will reduce the overall efficiency of the engine. In transformation 3-4, heat is rejected to the environment according to the following equation:

$$Q_c = M R^* T_{cold} \ln(r) \tag{12}$$

The overall work produced by the Stirling cycle is $W = Q_H - Q_C$. The efficiency of the ideal Stirling engine can be calculated as $\eta = W/Q_H$ and is usually very high as it is equal to the Carnot efficiency $1 - (T_{cold}/T_{hot})$. In reality, the efficiency is much lower since serval inefficiencies must be taken into account, such as that of the aforementioned regenerator, as well as mechanical and thermal losses.

Nominal sizing The Stirling engine was modeled considering the ideal cycle described above. In addition to the data presented in Table 2, information on the operating volume was needed. For this reason, it was assumed that the compression ratio of the engine was 1.5. This is a reasonable value for Stirling engines, considering that the maximum possible compression ratio is usually 2 [9]. The work produced by the cycle is:

$$W_{out} = MR^* T_{hot} \ln(r) + MR^* T_{cold} \ln(r) \tag{13}$$

It is possible to solve this equation for M, since everything else is known. To compute the value of V and P for every point of the cycle, the information about the mean pressure can be exploited. The mean pressure of the first and second isothermal transformation is computed using the mean value theorem:

$$f(c) = \int_a^b f(x)\,dx/(b-a) \tag{14}$$

Knowing that for an isothermal transformation:

$$PV = const. = MR^* T$$

The mean value theorem becomes, in this case:

$$P_{m,i} = \int_{V_a}^{V_b} \frac{MR^* T}{V}\,dV/(V_b - V_a) = \frac{MR^* T \ln(r)}{V_b - V_a} \tag{15}$$

Computing the mean pressure of the first and second isothermal transformation, $P_{m,1}$ and $P_{m,2}$ and imposing that $P_m = (P_{m,1} + P_{m,2})/2$, it is then possible to find the value of V_a and V_b. By applying this methodology, the whole cycle can be resolved for every model of the Stirling engine. The whole cycle for the three engines is shown in Figure 7. The main parameters, referring to the nominal case, of the three engines are shown in Table 7. It should be noted that only the mass and volume of the working fluid have been computed, while the mass and volume occupied by the engine itself are neglected. Despite this being a very strong approximation, as the majority of the mass and volume of the engine will be given by the engine itself, and not the working fluid, this method makes it possible to roughly classify the engines according to their mass and volume.

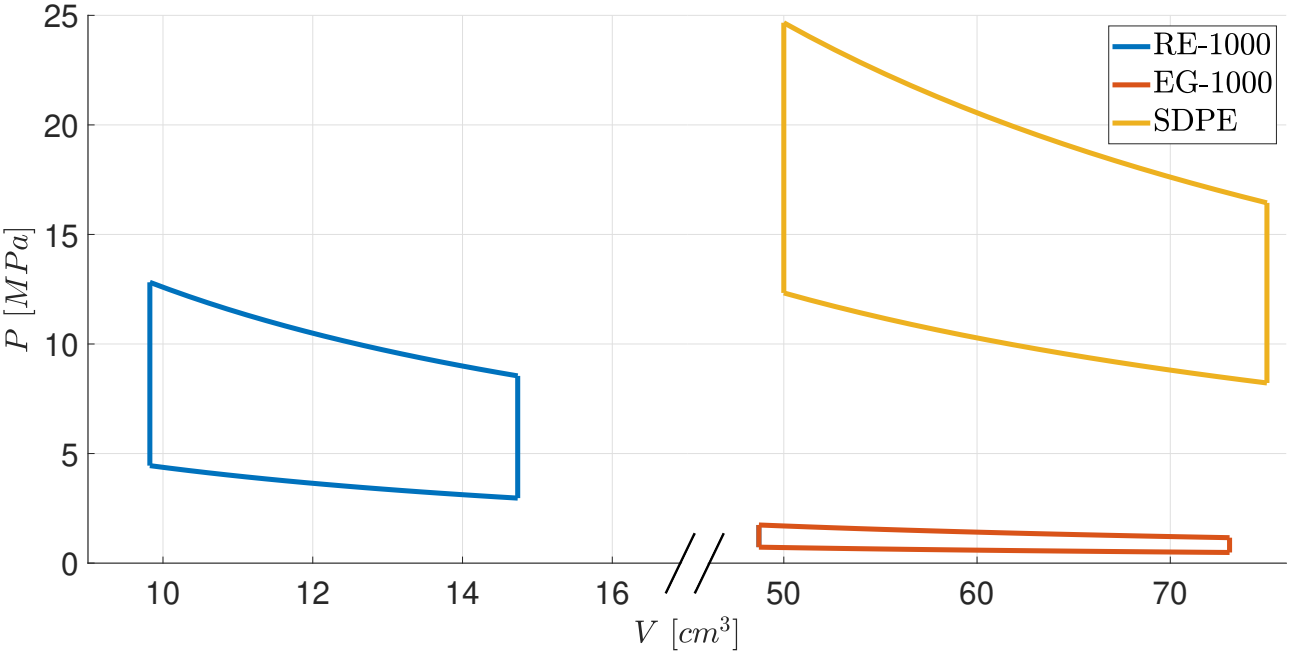

Figure 7: Stirling cycles on the $P-V$ diagram.

Parameter	RE-1000	EG-1000	SDPE
Working fluid mass $[kg]$	$6.94 \cdot 10^{-5}$	$5.27 \cdot 10^{-5}$	$9.13 \cdot 10^{-4}$
Total working fluid volume $[cm^3]$	14.74	73.07	75.0
Ideal Carnot efficiency [-]	0.6529	0.5821	0.50
Ideal input power $[kW_{th}]$ [1]	1.53	1.72	50
Real input power $[kW_{th}]$ [2]	3.45	5	113.64

Table 7: Main parameters of the three Stirling engines model.

From the table it is possible to notice that, since the reactor power is $5\,kW_{th}$, two RE-1000 are needed to manage all the heat of the core, bringing the total mass to $1.39 \cdot 10^{-4}\,kg$ and the volume to $29.48\,cm^3$. Therefore, in the nominal case, the RE-1000 is more convenient in terms of volume, while the EG-1000 is the best choice in terms of mass. To choose between the two, a more detailed set of requirements is needed.

2.1.5 Radiators

Radiators are designed to dissipate the thermal power output of 2.45 kW_{th} from the Stirling engine to the surrounding environment, maintaining a specified operating temperature. The Krusty reactor makes use of $Ti - H_2O$ heat pipes radiators. The heat pipes are constructed using titanium as the structural material, which is chosen for its high strength-to-weight ratio, corrosion resistance, and ability to withstand harsh thermal and mechanical conditions encountered during space missions. Attached to these heat pipes are aluminum radiator panels, which provide the surface area necessary for radiative heat dissipation into the space environment. The junction between titanium and aluminum is optimized using S-Bond technology, minimizing thermal resistance and addressing thermal expansion mismatches. The working fluid within the heat pipes is water, selected for its thermo-physical properties, particularly its high latent heat of vaporization [2]. The heat pipe operates based on a phase-change cycle:

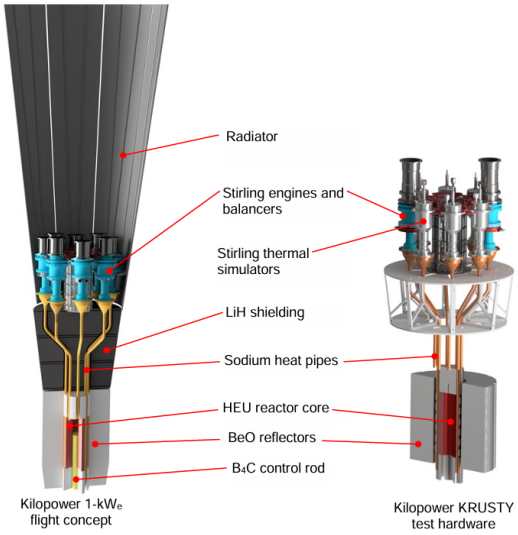

Figure 8: Krusty configuration [5]

1. At the evaporator section, waste heat from the Stirling converter causes the water to absorb thermal energy and evaporate, transforming into vapor.

2. The vapor travels through the heat pipe to the condenser section, where it releases heat by condensing back into liquid form. This heat is transferred to the aluminum panels and dissipated into space through thermal radiation.

3. The condensed water is then passively returned to the evaporator via capillary action facilitated by the internal wick structure.

A key feature of this system is the constant temperature maintained along the heat pipe during operation, allowing to consider also the temperature of the aluminum panels constant and so the heat is dissipated only through radiation. This is achieved because the heat transfer occurs primarily through the latent heat of vaporization and condensation, rather than through significant temperature gradients.

[1] Computed considering ideal Carnot efficiency.
[2] Computed considering real efficiency provided in the datasheets.

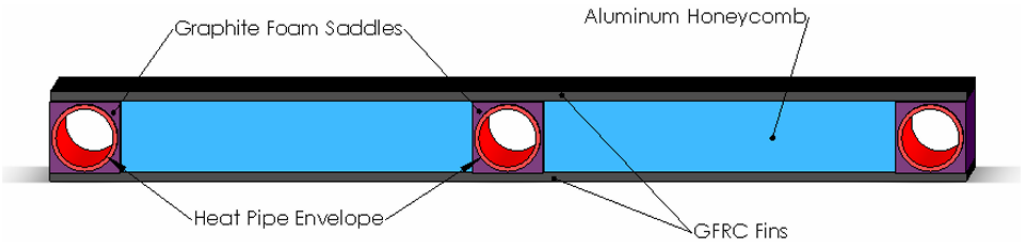

Figure 9: Heat Pipe Radiators [1]

To initiate the design process, a preliminary thermal analysis is conducted. The heat dissipation occurs through radiation to both deep space and the lunar surface, as previously said. To determine whether a Lumped Parameter Approach (LPA) can be applied and so neglect the variation of the temperature across the thickness, the Biot number is calculated. Since the radiation equations need to be linearized, the equivalent Newtonian convective heat transfer coefficient (h_{rad}) can be expressed as:

$$h_{rad} = \sigma(T + T_{ext})(T^2 + T_{ext}^2) \tag{16}$$

where σ is the Stephan-Boltzmann constant, T is the radiator's initial temperature, equal to the cold side temperature of the Stirling engine and T_{ext} is the environmental temperature, which is either $T_{DS} = 2.7\,K$ for deep space or $T_{LS} = 175\,K$ for the lunar surface. This formulation allows for a simplified calculation of the radiative heat transfer coefficients $h_{DS} = 1.59 W/m^2K$ and $h_{LS} = 3.32 W/m^2K$. At this point, the Biot number can be computed considering the parameters in Table 8.

Characteristic length [s]	Convective coefficient [h_{tot}]	Conductive coefficient [λ]
2.5 [mm]	4.41 [W/m^2K]	240 [W/mK]

Table 8: Biot number parameters.

The Biot number is $Bi = \dfrac{h_{tot}\,S}{\lambda}$, where the characteristic dimension is the thickness due to its definition as the ratio between the volume of the radiator and the wet area and the conductive coefficient is that of the aluminum as the face-sheet of the radiator. The final value of $Bi = 5.11 \cdot 10^{-5}$ confirms that the LPA method can be employed in this analysis (since it is lower than 0.1).
This considerations allow to make the hypothesis that, to compute the radiators area needed to dissipate the thermal power coming from the Stirling engine, can be considered only the heat transfer due to radiation, neglecting the conduction. The thermal power is then dissipate according to the following equation:

$$Q_{\text{diss}} = A_{\text{rad}} \left[\sigma \left(\varepsilon_r \left(T_{\text{hot,r}}^4 - T_{\text{DP}}^4\right) + \varepsilon_r \left(T_{\text{hot,r}}^4 - T_{\text{LS}}^4\right) - \alpha_r E_{\text{Sun}} \sin\phi\right)\right] \tag{17}$$

where σ is the Stephan-Boltzamann constant, $\varepsilon_r = 0.86$ and $\alpha_r = 0.2$ are respectively the values of emissivity and absorbance for space radiators [11]. $T_{\text{hot,r}} = 303K$ is the hot side radiators temperature (that corresponds to the cold side of the Stirling engine), $E_{Sun} = 1350 W/m^2$ is the irradiance power of the Sun and $\phi = 2^o$ is the maximum inclination of the solar rays on the radiators [11], considering the lunar south pole. Solving the equation an area of $2.24\,m^2$ is obtained.

2.2 Parametric Analysis

There is no need to perform a sensitivity analysis in this case, as the radiator dimensions are fixed and remain unaffected by variations in other parameters, making additional evaluations unnecessary.

2.2.1 Heat Pipes

It is necessary to assess the behavior of the heat pipes diameter for growing core thermal power, from $5\,kW_t$ to $50\,kW_t$. In particular, keeping the same configuration (8 pipes) is necessary to determine which physical constrain limits the pipes diameter. Using the procedure shown in subsubsection 2.1.3, the following **??** is obtained:

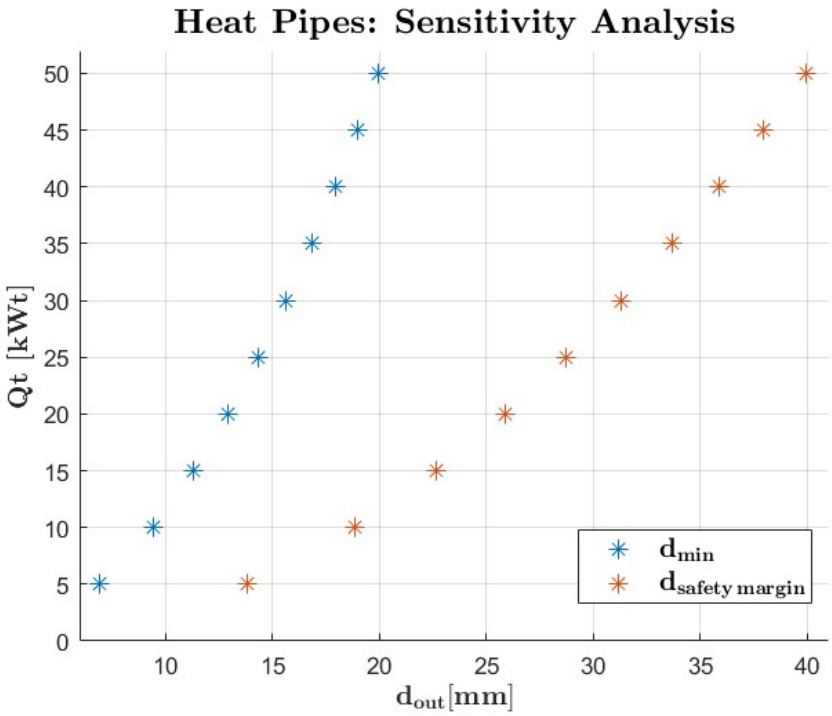

Figure 10: Heat pipes pipes diameter for varying core thermal power

As expected, the outer diameter grows with the core thermal power and the limit is set for all the analysed cases by the entrainment thermal power. The entrainment limit in KRUSTY heat pipes is the most restrictive constraint, as it directly limits heat transport by preventing liquid return to the evaporator. As thermal power increases, the rising vapor velocity intensifies droplet entrainment, leading to wick dry-out and potential heat pipe failure. This effect persists across varying core thermal powers, making entrainment the dominant limitation. In contrast, the sonic limit, which occurs when vapor reaches the speed of sound, is not a concern under KRUSTY's operating conditions. The viscous limit only affects low-temperature, low-power regimes, which are irrelevant for KRUSTY. While the boiling limit can cause local dry-out, it is mitigated by proper wick design and liquid management, leaving entrainment as the primary constraint on thermal performance. A 100% safety limit on the diameter is adopted to assure proper behavior and to remove small inaccuracies due to the simplifying assumptions.

2.2.2 Stirling

To analyze which Stirling engine model is more convenient as the power output of the core varies, a brief analysis is performed. By changing the power of the core, it is possible to compute and plot the overall mass and volume of the engines, accounting for the number of engines needed to manage the output power of the reactor. The results are shown in Figure 11.

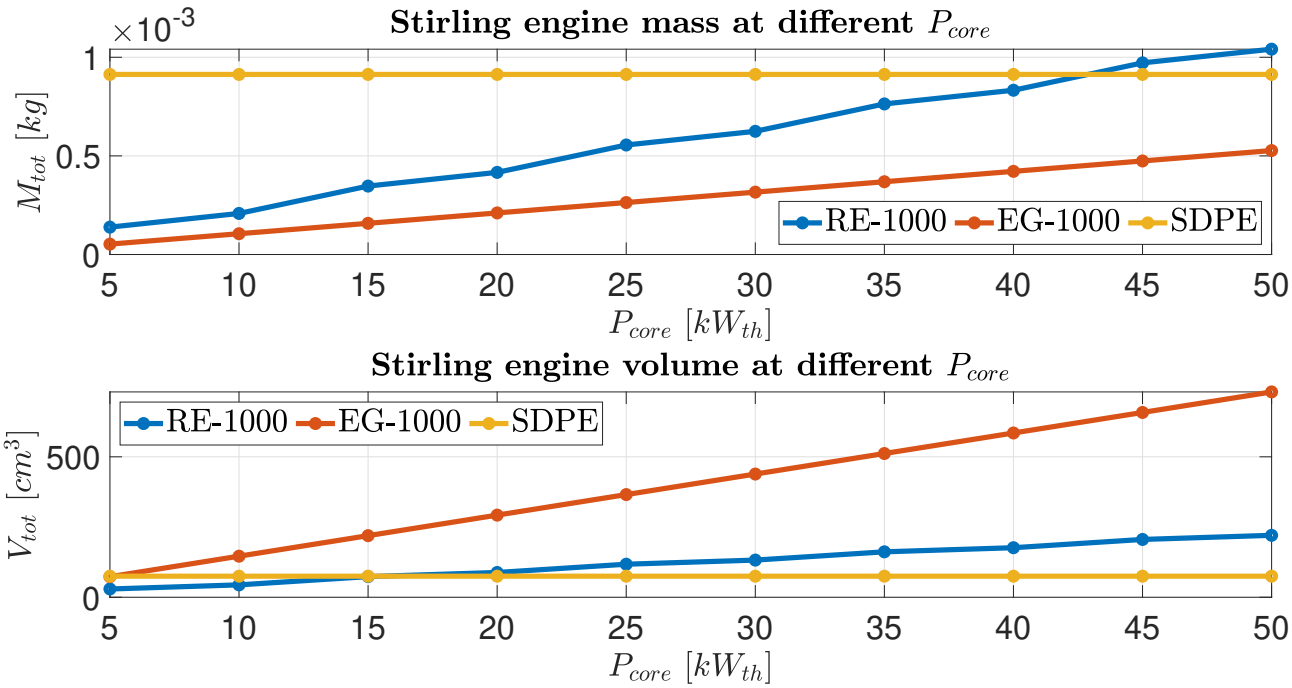

Figure 11: Total mass and volume of Stirling engines at different core power outputs.

From the plot, it is evident that no engine is clearly better than the others. If the requirement on weight is more stringent than the on volume, then it is always better to choose the EG-1000, otherwise, it is more convenient to choose the RE-1000 up to a power level of about $15\,kW$, where the SDPE is the most compact. For this reason, to choose which one is better for the mission, a more detailed set of requirements is needed.

3 Conclusions

In conclusion, the KRUSTY reactor design effectively addresses the power generation needs for a lunar base. The reactor's use of highly enriched Uranium-235 and liquid sodium, along with Stirling engines, ensures reliable power in the absence of sunlight. The analysis confirms that the reactor meets key mission requirements, such as continuous operation for up to 12 years and resilience in the harsh lunar environment. The trade-off analysis of Stirling engines indicates that the RE-1000 and EG-1000 models are suitable, with the choice depending on specific mission constraints related to mass and volume. The heat pipe sizing, constrained primarily by the entrainment limit, and the radiator design, optimized for radiative heat dissipation, ensure efficient thermal management. Overall, the KRUSTY reactor design is well-suited for its intended application, providing a robust solution for sustained lunar operations.

References

[1] William G. Anderson, David B. Sarraf, Scott D. Garner, and Jim Barth. "High Temperature Titanium-Water Heat Pipe Radiator". In: *American Institute of Aeronautics and Astronautics* (2006). NASA Glenn Research Center, Contract NNC04CA32C and NNC05TA36T, pp. 1–9. DOI: 10.1063/1.2169184. URL: https://www.researchgate.net/publication/259668117_High_Temperature_Titanium-Water_Heat_Pipe_Radiator.

[2] Thomas Godfroy Patrick R. McClure David I. Poston Marc A. Gibson. "KRUSTY Reactor Design". In: *https://www.tandfonline.com/loi/unct20* (2020). DOI: https://doi.org/10.1080/00295450.2020.1725382.

[3] J.K. Fink. *Tables of thermodynamic properties of sodium*. June 1982. DOI: http://dx.doi.org/10.2172/6856038.

[4] F. Franks. *Water, A Matrix of Life, 2nd Ed.* The Royal Society of Chemistry, 2000. DOI: https://doi.org/10.1039/9781847552341.

[5] Marc A. Gibson, David I. Poston, Patrick McClure, Thomas J. Godfroy, Maxwell H. Briggs, and James L. Sanzi. *Kilopower Reactor Using Stirling Technology (KRUSTY): Nuclear Ground Test Results and Lessons Learned*. Tech. rep. NASA/TM-2018-219941. Technical Memorandum. Cleveland, Ohio: NASA Glenn Research Center, Oct. 2018. URL: http://ntrs.nasa.gov/.

[6] Joshua Hansel, Ray Berry, David Andrs, and Richard Martineau. *Sockeye Theory Manual*. Mar. 2020. DOI: http://dx.doi.org/10.2172/1697979.

[7] Joshua E. Hansel, Carolina da Silva Bourdot Dutra, Lise Charlot, and Elia Merzari. "The liquid-conduction, vapor-flow heat pipe model in Sockeye". In: *Nuclear Engineering and Design* 426 (Sept. 2024), p. 113359. ISSN: 0029-5493. DOI: http://dx.doi.org/10.1016/j.nucengdes.2024.113359.

[8] Kuan-Lin Lee, Calin Tarau, and William G. Anderson. "Titanium Water Heat Pipe Radiators for Space Fission System Thermal Management". In: *Joint 19th IHPC and 13th IHPS*. NASA Glenn Research Center research. Advanced Cooling Technologies, Inc. Pisa, Italy, 2018.

[9] K. Mahkamov. "Thermal-engine-based small and micro combined heat and power (CHP) systems for domestic applications: modelling micro-CHP deployment". In: *Small and Micro Combined Heat and Power (CHP) Systems*. Elsevier, 2011, pp. 459–509. ISBN: 9781845697952. DOI: https://doi.org/10.1533/9780857092755.3.459.

[10] N. Meyer. "Simulation numérique de la viscosité de liquides : effets des paramètres d'interaction, de la température et de la pression sous conditions ambiantes et extrêmes". MA thesis. Université de Lorraine, 2017. URL: https://theses.hal.science/tel-01810298v1.

[11] C. Molteni. "Preliminary architecture of nuclear space reactor for a lunar base". MA thesis. Politecnico di Milano, 2022. URL: https://hdl.handle.net/10589/191597.

[12] I. Pioro and R. Duffey. "Current and future nuclear power reactors and plants". In: *Managing Global Warming*. Elsevier, 2019, pp. 117–197. ISBN: 9780128141045. DOI: https://doi.org/10.1016/B978-0-12-814104-5.00004-1.

[13] Varley F. Sears. "Neutron scattering lengths and cross sections". In: *Neutron News* 3.3 (Jan. 1992), pp. 26–37. ISSN: 1931-7352. DOI: https://doi.org/10.1080/10448639208218770.

[14] Jian-song Zhang, Hua-ping Mei, Yong-ju Sun, Sheng-qin Ma, and Tao-sheng Li. "Design of high-temperature sodium heat pipe with composite wick based on non-dominated sorting genetic algorithm (NSGA)". In: *Nuclear Engineering and Technology* (Oct. 2024), p. 103260. ISSN: 1738-5733. DOI: http://dx.doi.org/10.1016/j.net.2024.10.022.